Mg^2+ Ion Doping in Copper Nanoferrite Material For Microwave Absorption Application

Kumar, Sanjay
Electrical Engineering Department, National Institute of Technology Kurukshetra

Dewan, Lillie
Electrical Engineering Department, National Institute of Technology Kurukshetra

https://doi.org/10.5109/7183320

出版情報：Evergreen. 11 (2), pp.632-639, 2024-06. 九州大学グリーンテクノロジー研究教育センター
バージョン：

Mg^{2+} Ion Doping in Copper Nanoferrite Material For Microwave Absorption Application

Sanjay Kumar[1*], Lillie Dewan[1]
[1]Electrical Engineering Department,
National Institute of Technology Kurukshetra, India 136119

*E-mail: sanjaykkr25@gmail.com

(Received October 04, 2023; Revised March 27, 2024; accepted April 19, 2024).

Abstract: In this paper properties of magnesium doped copper ferrite are evaluated and it is often that suitable for microwave absorption application. Soft $Mg_xCu_{1-x}Fe_2O_4$ ferrite nanoparticles were synthesized by using simple chemical co-precipitation technique at 90^0C. The structural details and characterization is portrayed by utilizing powder XRD, FTIR, HRTEM, EPR and VSM procedures. XRD examples affirmed the single-stage cubic spinel structure of nanoparticles with no additional stage and crystalline size lies in the range 8-20 nm. It was observed that the lattice parameter diminishes with expanding cation substitution of Mg^{2+}. EPR spectra of the considerable number of tests show a ferromagnetic single broad resonance signal shifts to the higher field on increasing Mg ions concentration.

Keywords: Lattice parameter; co-precipitation; maximum magnetization; dielectric constant.

1. Introduction

Properties of nanomaterials largely depend on crystallite size, nature of dopant, doping concentration and distribution of dopant ions. Different routes sol-gel, co-precipitation, solid state reaction method etc. have been followed to synthesize magnetic nanoparticles as it has an important role in deciding the properties of ferrites[1–5]. Ferrite magnetic nanoparticles due to their good microwave absorption property are used to create invisibility of the air vehicles to the radar signals which is known as stealth technology which aims to make an air and ground vehicles invisible to radar.

For microwave absorption property dielectric composites may possibly comprise mixed ferrites to augment the magnetic and dielectric properties of a material. In $CuFe_2O_4$ a highly magnetic ferrite, Cu^{2+} ions occupy B sites and hence, have completely inverse spinel structure[6] and in $MgFe_2O_4$, Mg^{2+} ions preferably occupy B sites, leads to the formation of partially inverse spinel structure[7]. $MgFe_2O_4$ have been a material of great interest in the field of Ferro fluids, transformers, humidity and gas sensing, catalysis etc. due to low dielectric losses and high resistivity[8]. Kavita verma et al. reported the effect of Mg ion doping in Cu ferrite materials which have high dielectric properties[9]. Novel Mg doped Zn-Li spinel ferrites of various compositions have been prepared by sol-gel auto combustion technique[10]. The dielectric properties of Poly crystalline spinel ferrite $Ni_{1-x}Mg_xFe_2O_4$ (x= 0, 0.1, 0.3, 0.5, 0.7) nanoparticles has been synthesized by the co-precipitation method in[11]. $Ni_{1-x}A_xFe_2O_4$ (A =Zn, Mg and x =0.0, 0.5) has been prepared by chemical co-precipitation method with a motivation to seek the role of nonmagnetic Zn and Mg doping on structural and dielectric properties of $NiFe_2O_4$ has been studied in [12]. The samples of $A_xCo_{1-x}Fe_2O_4$ (A = Zn, Mg and x = 0.0, 0.5) were successfully prepared by chemical co-precipitation method in [13].

Recently, intrinsic properties of copper ferrites have been enhanced by using doping effect by various researchers. Substitution of various metal ions like Zn^{2+}, Co^{2+}, Nd^{3+}, Yb^{3+}, La^{3+}, Sm^{3+} and Gd^{3+} etc. has been studied to investigate the effect on structural magnetic and electrical properties of copper ferrites, La_2NiMnO_6 based Perovskite solar cells, photovoltaic performance investigation of $Cs_3Bi_2I_9$ based, low-temperature synthesis of potassium triniobate (KNB_3O_8), and simple−cubic−perovskite ($Ba_{0.62}K_{0.38}$)[14–21]. But still, the authors did not acknowledge the synthesis of Mg^{2+} ion doped copper ferrite so far. In the present work, to modify electrical and magnetic property of copper ferrites, doping effect of Mg^{2+} ion of copper ferrites has been studied for microwave absorption application. It has been found after the synthesized the material that material has excellent structural properties, High-Saturation magnetization, good dielectric properties variation with frequency, microwave absorption property, which often advantage performance over their structure.

In this work, Mg doped $CuFe_2O_4$ have been synthesized using co-precipitation method. Detailed structural studies have been investigated using XRD, FTIR, HRTEM, VSM and EPR. Variation in magnetic properties with

replacement of Cu^{2+} ions with Mg^{2+} ions is inspected using VSM.

Main focus of this study is to explore the dielectric properties with increase in doping of Mg^{2+} ions and to use them for microwave absorption application. Unfortunately, there is currently not much of an exhaustive study that provides information on the optical and magnetic properties of nanostructures of $Mg_xCu_{1-x}Fe_2O_4$ doped with Mg^{2+}. Furthermore, there has been no previous publication on a thorough investigation of the structural, morphological, optical, and magnetic characteristics of Mg^{2+}-doped $Cu_{1-x}Fe_2O_4$ nanostructures that has been generated using the co-precipitation process. In this study, the precipitation approach has been used to synthesize a range of $Mg_xCu_{1-x}Fe_2O_4$ (x = 0.1, 0.2, 0.3, 0.4, and 0.5) nanoferrites. A study has been conducted to examine the influence of adding magnesium ions on the structural, optical, and magnetic characteristics of $Cu_{1-x}Fe_2O_4$ nanoparticles. The study provided novel optical characteristics of $Mg_xCu_{1-x}Fe_2O_4$ nanoferrites.

This paper is organized as follow: Discuses the brief introduction in section 1. Experimental synthesis of the Mg-Cu ferrites nanoparticles is detailed in Section 2. Characterization of the material by different methods and results are discussed in Section 3. Finally, the conclusion is summarized in Section 4 followed by references and Acknowledgements.

2. Experimental

Facile substance co-precipitation strategy is used to produce Mg^{2+} particle doped Mg-Cu ferrites nanoparticles with composition $Mg_xCu_{1-x}Fe_2O_4$ $(0.1\leq x\leq 0.5)$. High immaculateness AR grade Merck synthetic salts of $Mg(NO_3)_2.6H_2O$, $Cu(NO_3)_2.6H_2O$ and $Fe(NO_3)_3.9H_2O$ were utilized as beginning materials for the production.

Step A:- The homogeneous solutions of these salts were blended in stoichiometric proportion.

Step B:- 25 % Ammonia solution was drop shrewd to keep pH consistency 9.0 of solution mixture.

Step C:- To avert particles agglomeration the individual particles during precipitation are surfactant using Oleic acid.

The arrangement of ferrite nanoparticles happens in two-advance procedure:

1. Co-precipitation step:

Metal salts have been changed over into hydroxides (at 90^0C)

$$x\mathrm{Mg}^{2+} + (1-x)\mathrm{Cu}^{2+} + 2\mathrm{Fe}^{3+} + 8\mathrm{OH}^- \longrightarrow x\mathrm{Mg(OH)_2}.(1-x)\mathrm{Cu(OH)_2}.2\mathrm{Fe(OH)_3} \quad (1)$$

2. Ferritization step:

Hydroxides converted into Nano ferrites.

$$x\mathrm{Mg(OH)_2}.(1-x)\ \mathrm{Cu(OH)_2}.2\mathrm{Fe(OH)}^-_3 \longrightarrow \mathrm{Mg_xCu_{1-x}Fe_2O_4} + 4\mathrm{H_2O} \quad (2)$$

The precipitated particles were cleaned 4-5 times with double distilled water for washout salt deposits and other contaminations and then dried at 90^0C to get the powder.

3. Characterizartion of Material

This section contains synthesized materials which are characterized by XRD, FTIR, HRTEM, EPR and VSM. The dielectric property of this material is also discussed in the section.

A. XRD Pattern

To diagnose the phase of a crystal at room temperature XRD patterns for the desired compositions i.e. . $Mg_xCu_{1-x}Fe_2O_4$ (x= 0.1- 0.5) have been taken using model 'Rigaku Make Powder'[22] operating at a wavelength of 1.5406 Å. Figure 1 shows pure crystalline nature of the compositions with no additional peak. The crystalline size obtained from Debye's relation and the calculated structural factors are given in Table I and all samples are single-phase cubic spinel structure. The variation of lattice parameters and crystallite size is shown in Fig. 2. It can be seen that the lattice parameter values go on diminishing with increasing Mg^{2+} ions at ease in the copper ferrite particles, as smaller radii (0.66 Å) magnesium ions are substituting larger radii (0.82 Å) copper ions. Crystalline size is found to be in the range 7-14 nm and the variation in crystallite size can be attributed to the synergistic effect during annealing. The strain induced in the ferrite nanoparticles as the imperfections in the material emanate with doping and can be evaluated from W-H relation[23] given by:

$$\beta_{hkl} = \frac{k\lambda}{D\cos\theta} + 4\epsilon\tan\theta \quad (3)$$

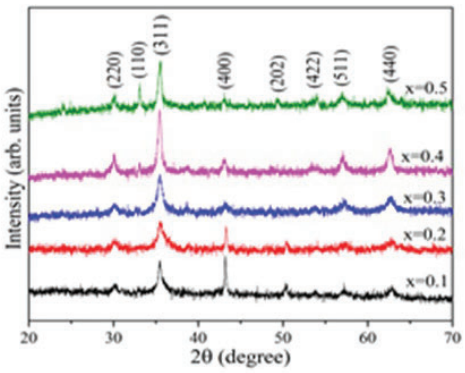

Fig.1. XRD Patterns of synthesized $Mg_xCu_{1-x}Fe_2O_4$ samples (x= 0.1, 0.2, 0.3, 0.4 and 0.5)

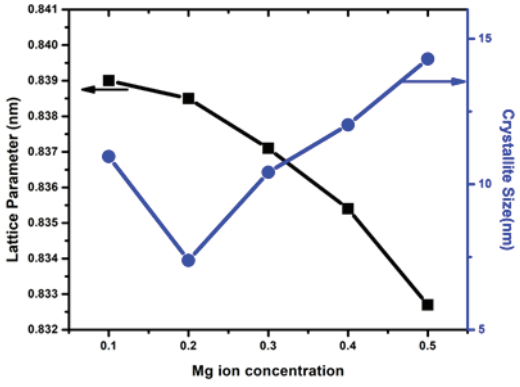

Fig. 2. Variation of lattice parameter and crystallite size with Mg^{2+} ion concentration

Table I: Various structural parameters of $Mg_xCu_{1-x}Fe_2O_4$ (x= 0.1, 0.2, 0.3, 0.4, 0.5) samples.

Sample	D (nm)	d (Å)	a(Å)	r_A(Å)	r_B(Å)	L_A(Å)	L_B(Å)
x=0.1	10.95	2.523	8.370	0.4900	0.7725	3.624	2.959
x=0.2	7.38	2.516	8.345	0.4846	0.7663	3.613	2.950
x=0.3	10.41	2.525	8.376	0.4913	0.7740	3.627	2.961
x=0.4	16.04	2.528	8.387	0.4936	0.7767	3.631	2.965
x=0.5	17.03	2.526	8.378	0.4917	0.7745	3.627	2.962

B. FTIR Pattern

Infra-red spectra of the compositions were recorded with FTIR 'NICOLET 5700' spectrometer. Fourier transform infrared spectra of the prepared composition in the 400 – 4000 cm^{-1} region are outlined in Fig. 3.

The larger frequency band lies in 550-565 cm^{-1} region shows the Mt – O stretching vibes at tetrahedral locus.

Fig.3. FTIR Spectra of $Mg_xCu_{1-x}Fe_2O_4$

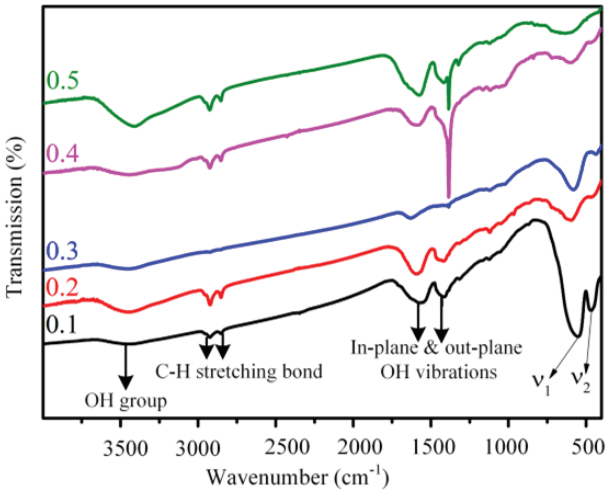

samples(x= 0.1, 0.2, 0.3, 0.4 and 0.5)

The other band of low frequency lies in 405-420 cm^{-1} region shows the Mo – O stretching vibes at octahedral locus. The gap in the positions of two bands arise due to variation in M-O width at A and B sites[24]. These absorption bands manifest the crystalline spinel network of prepared compositions. With rise in magnesium ion content Mt – O band shift towards the larger wave number. This shift in wave number signifies that the tetrahedral complexes are also being preferred by Mg ions. Hence magnesium ions reside at both tetrahedron and octahedron complexes as reported by[25]

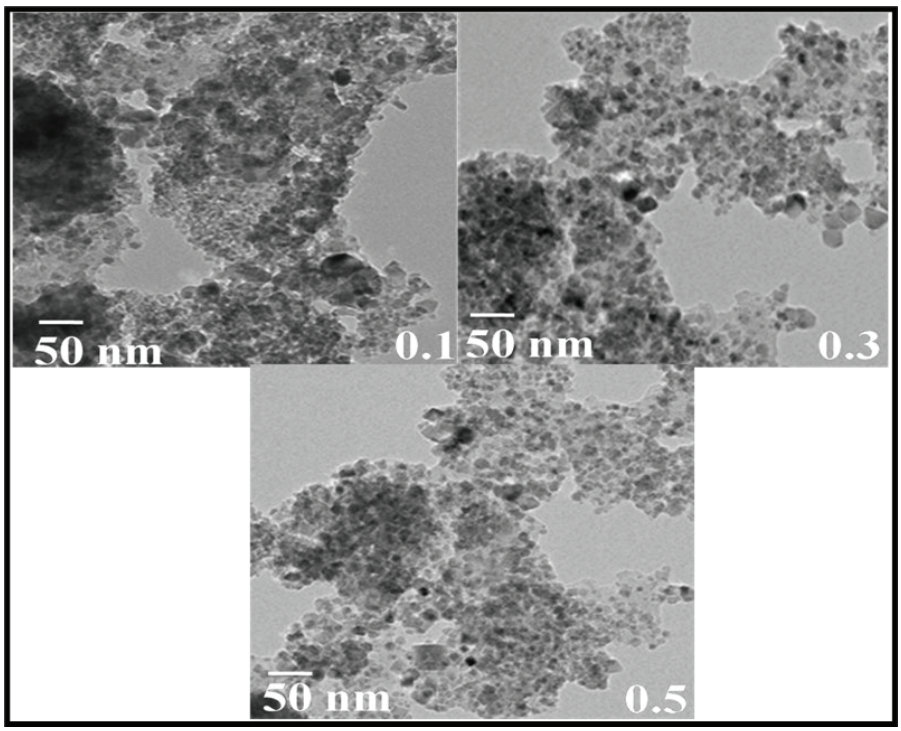

Fig. 4. HR-TEM images and histogram of $Mg_xCu_{1-x}Fe_2O_4$ (x = 0.1, 0.3 and 0.5) nanoparticles

C. High-Resolution Transmission Electron Microscopy Pattern

Structural micrographs of the samples were taken using 'Tecnai G20' HRTEM microscope. To check the particle size and morphology HR-TEM images of manufactured $Mg_xCu_{1-x}Fe_2O_4$ nanoparticles have been shown in Fig. 4. Most of the particles are appearing to be spherical in nature with some agglomeration in magnetic nanoparticles. Average partcle size has been calculated by measuring the length of 30-50 nanoparticles randomly and found to be 12.6, 16.8 and 18.1 nm for samples with x = 0.1, 0.3 and 0.5 respectively. It is obsreved that particle size is reducing with increase in doping concentration of Mg content, since, ionic radius of Mg^{2+} ions (0.66 Å) is smaller that Cu^{2+} ions (0.73 Å).

D. Vibrating Sample Magnetometer

Magnetic parameters were estimated from vibrating sample magnetometer (VSM) recorded hysteresis loops at room temperature in -10 KOe to +10 KOe magnetic field range. Figure 5 shows change in magnetization on varying the applied magnetic field. It can be seen from figure that magnetization is not saturated decreases with increase in Mg content from 0.1 to 0.5. Maximum magnetization varies from 22.22 emu/gm for x = 0.1 to 15.65 emu/gm for x = 0.5. Magnetization decreases due to cation distribution of Cu and Mg cations $[Fe^{3+}]_T$ $[Cu_{1-x}^{2+}Mg_x^{2+}Fe^{3+}]O_4$.

The value of squareness, anisotropy constant and magnetic moment of the particles were calculated [11] by using formulas are given below;

$$K = \frac{H_c M_s}{0.96} \quad (4)$$

$$S = \frac{M_r}{M_s} \quad (5)$$

$$\eta_B = \frac{MW \times M_s}{5585} \quad (6)$$

where M , M_s , H_c and MW are the retentivity, maximum magnetization, coercivity and molecular weight of composition (in gm) respectively and magnetic factor is 5585

Table 2: Magnetic measurement of $Mg_xCu_{1-x}Fe_2O_4$ (x= 0.1, 0.2, 0.3, 0.4, 0.5) samples

Sample	M_s (emu/gm)	H_c (Oe)	M_r (emu/gm)	(S)	Anisotropy constant (K)	Bohr magneton (μ_B)
x=0.1	22.22	0.032	1.406	0.063	0.740	0.9361
x=0.2	21.18	0.009	0.323	0.015	0.202	0.8774
x=0.3	20.48	0.032	0.918	0.044	0.687	0.8339
x=0.4	17.66	0.035	1.097	0.062	0.643	0.7067
x=0.5	15.65	0.107	2.332	0.063-0.149	1.752	0.6153

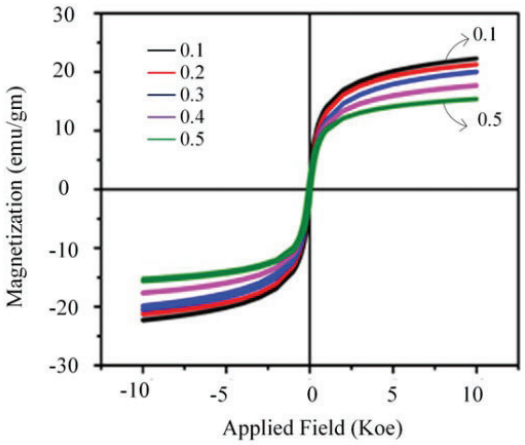

Fig. 5. Magnetization curve of $Mg_xCu_{1-x}Fe_2O_4$ samples (x= 0.1, 0.2, 0.3, 0.4 and 0.5)

A continuous decrease maximum magnetization value values in with Mg content can also be attributed to its non-magnetic behaviour. Furthermore, Mg^{2+} ions are smaller than that of Cu^{2+} ions, hence, has high surface to volume ratio which tend to increase the canted spins on the surface. These canted spins work as dead layers that do not contribute to magnetization. Therefore, a decrease in magnetization is observed with Mg content. Values of coercive field and retentively are almost found to be increased with Mg contribution.

E. Electron paramagnetic Resonance Pattern

Electron paramagnetic Resonance (EPR) spectroscopic exploration of ferrites throws light on their magnetic properties behavior at high frequency. EPR spectra of $Mg_xCu_{1-x}Fe_2O_4$ (x = 0.1, 0.2, 0.3, 0.4, 0.5) samples recorded on M/S Bruker Biospin A300 X-band EPR Spectrometer at 9.85 GHz microwave frequency and 100 kHz modulation frequency are broad resonance signal arising from the spin and electromagnetic waves interaction shown in Fig 6. EPR parameters like peak-to-peak line width (ΔH_{pp}), half peak width ($\Delta H_{1/2}$), g-value, spin concentration (spin/g) and spin-spin relaxation time constant (τ_2) (sec.) are derived by considering Lorentzian distribution using the following relations and listed in Table 3.

$$g - value = \frac{hv}{\mu_B H_r} \quad (7)$$

$$\Delta H_{1/2} = \sqrt{3}\Delta H_{pp} \quad (8)$$

$$\tau_2 = \frac{h}{2\pi g \mu_B \Delta H_{1/2}} \quad (9)$$

where h: Planck's Constant, μ_B: Bohr Magneton, ν: Microwave Frequency, Hr: Resonance Magnetic Field, g: g-value, $\Delta H_{1/2}$: Half Peak-to-Peak Line width ΔHpp value of these broad resonance signals varies with Mg2+ ions concentration in the range from 650 G to 875 G.

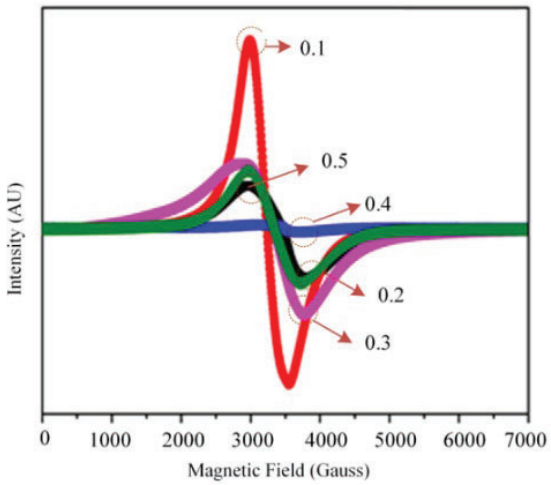

Fig. 6. EPR spectra of $Mg_xCu_{1-x}Fe_2O_4$ samples with different Mg^{2+} ion concentration recorded at room temperature.

First increase and then decrease in peak -to- peak line width on increasing Mg concentration is attributed to the change in crystalline field effect and reduction in magneto crystalline anisotropy [26]. The narrow resonance line width exhibits better magnetic field homogeneity among ferrite nanoparticles[27].

Table 3: EPR Measurement of $Mg_xCu_{1-x}Fe_2O_4$ samples with different Mg^{2+} ion concentration

Sample	H_R (G)	ΔH_{PP} (G)	g-value	N_s (spin/g)	Spin-Spin Relaxation time Constant (sec)
x=0.1	3233.78	567.04	2.1376	4.56×10^{15}	5.42×10^{-15}
x=0.2	3333.05	850.54	2.0739	5.42×10^{15}	3.72×10^{-15}
x=0.3	3352.60	749.03	2.0618	1.71×10^{16}	4.25×10^{-16}
x=0.4	3442.84	676.84	2.0078	4.48×10^{15}	4.83×10^{-15}
x=0.5	3475.14	625.80	1.9891	1.98×10^{15}	5.27×10^{-15}

In doped ferrites, the dipolar-dipolar and super-exchange interactions play vital role which broadens and narrows down the resonance signal respectively[28]. It means Mg doping weakens super-exchange interaction in x = 0.2 case and then improves on further increasing Mg concentration in samples. In super-exchange interactions, the moments of A site ions align anti parallel or parallel to B site ions to increase or reduce the internal field respectively[29]. The resonance field (Hr) value shifts to higher magnetic field on increasing Mg content. Hr value of first derivative EPR signal depends upon the anisotropy, porosity, non-uniform demagnetization, maximum magnetization and internal field parameters[26]. In the present case substitution of non-magnetic Mg^{2+} at Cu^{2+} ions site reduces the internal field and shift resonance to higher magnetic field with increasing Mg content to fulfill resonance condition i.e. hν = gβHr. g- value decreases from 2.1376 to 1.9891 on increasing Mg content because it is inversely proportional to the resonance field value, as per Equation (8) and also due to low magneto-crystalline anisotropy. The spin concentration of these samples is calculated by the comparison method where DPPH has been used as standard reference material. The spin-spin relaxation time constant are calculated by using equations (8-9). These derived EPR parameters are also supported by the inferences drawn from magnetic studies made by VSM in the present series of Mg doped samples.

F. Dielectric Properties

Dielectric behaviors of the composition has been studies using Impedance Analyzer. The variation in dielectric constant with frequency for all the samples are outlined in Fig.7. At low frequencies, the value of dielectric constant goes on decreasing with increasing frequency while it becomes independent at larger frequencies. This behavior is explained in terms of "Maxwell – Wagner" model [30]. Accordingly, ferrites structure presumed to consist of largely conducting modes (grains) embedded in insulating mold (grain boundaries) [31]. In low frequency zone these boundaries are highly active and with increase in frequency the conducting grains play their role results in decrease in the dielectric constant. This can be interpreted in terms of polarized space charge that occurred because of highly conducting grains present between insulating boundaries. The exchange of Fe^{3+} ions and Fe^{2+} ions, results displacement along the applied field contribute in polarization. Hence dielectric constant becomes high at small frequency.

The graph between dielectric loss and frequency for synthesized samples are shown in Fig. 8. It is seen that, the value of loss goes on decreasing with rise in frequency often certain range of frequency. If the hopping frequency of electron at B-site is larger than the applied field frequency, the electrons will trail the field with maximum loss. At large frequencies hopped electrons among ferric and ferrous ions not retain pace with field applied causing a reduction in contribution of polarized space charge as a result of which reduction in dielectric loss is observed. At small frequencies dielectric loss possess large value because of the larger resistivity of the boundaries that

requires high energy to exchange electrons among ferric and ferrous ions.

The dielectric lose factor is represented as:

$$\tan\delta = \frac{\text{Energy dissipated in a dielectric material}}{\text{Energy stored in a dielectric material}} \quad (10)$$

OR

$$\tan\delta = \frac{\varepsilon''}{\varepsilon'}$$

and

$$\varepsilon'' = \varepsilon' \tan\delta \quad (11)$$

Is the phase different between applied field and induced current.

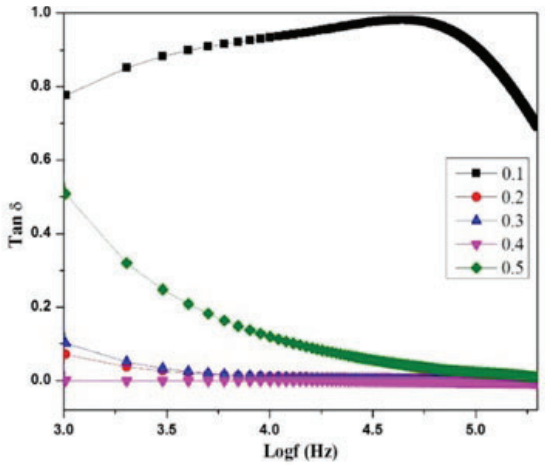

Fig.7. Variation of dielectric constant with frequency of $Mg_xCu_{1-x}Fe_2O_4$ samples

The AC conductivity of the synthesized samples with frequency is outlined in Fig. 9. It can be analyzed that at low frequencies the overall conductivity remains almost constant, rises slowly at intermediate region and get scattered at large frequencies. It is a fact that with rise in frequency, the conductivity of the compositions increases and explained with hopping model. At low

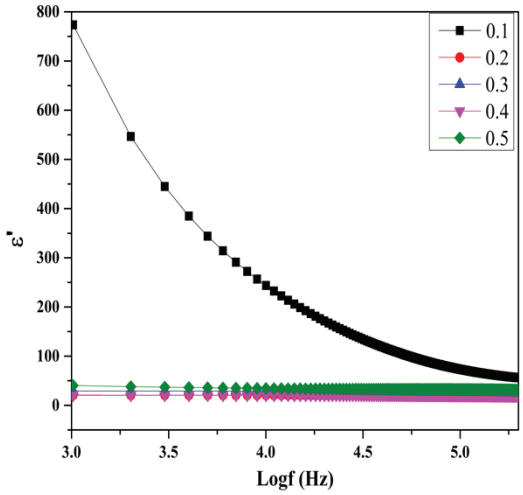

Fig. 8. Variation of dielectric loss with frequency of $Mg_xCu_{1-x}Fe_2O_4$ samples

frequency large resistance of the boundaries is highly effective and hence a plateau is obtained. At larger frequency the conductivity rises because of grain impact and of increase in hopping of carriers among ferric and ferrous ions at octahedron complex. The conductivity falls on adding Mg^{2+} ions because its oxidation state is stable and hence do not take part in conduction. Moreover, these ions inhibit the conduction among Fe^{3+} and Fe^{2+} ions by

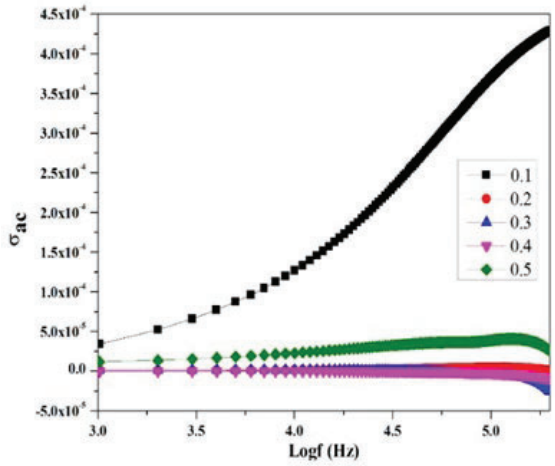

preferably residing at octahedron complex.

Fig. 9. Variation of ac conductivity with frequency of $Mg_xCu_{1-x}Fe_2O_4$ samples

4. Conclusion:

The magnesium ions doped copper nanomaterials have been prepared successfully using chemical co-precipitation approach to study the impact of magnesium substitution in altering the structural, optical, and magnetic properties of copper ferrites. X-ray diffraction patterns confirm the crystalline nature of the prepared materials. The size obtained using Debye relation raises from 10 to 20 nm. FTIR curves shows that the Mg ions get incorporated in the copper ferrite sample. TEM patterns provide the nanocrystalline nature of the sample and the nanoparticles form sphere and get clustered as a result of magnetic interactions. On substituting magnesium ions, the increase in magnetic factors such as M_s, H_c, S, K and M_r is observed. The decrease in dielectric factors such as dielectric loss, dielectric constant and AC conductivity is seen with rise in magnesium ion content which are suitable in microwave absorption applications. The produced nanoparticles have modified and adjustable magnetic characteristics, which may have significant applications. The features of doping of Mg^{2+} ion can be further explored by varying the constituted parameter of ferrites.

Appendix

Equipment used for characterized the material.

- X-ray diffraction pattern were recorded using 'Rigaku Make Powder' X-ray diffractometer.
- Infra-red spectra of the compositions were recorded With FTIR 'NICOLET 5700' spectrometer.
- Structural micrographs of the samples were taken using 'Tecnai G20' HRTEM microscope.
- VSM- Model ADE-EV was used to explore magnetic properties.
- EPR spectrum was recorded on Bruker Biospin Make, Model A300.
- The dielectric measurements were recorded by using HP4284A LCR meter attached with a lakeshore 340 temperature controller

Acknowledgement

The author acknowledges the technical support extended by Dr. Ashok Kumar Department of Physics, Deenbandhu Chhotu Ram University of Science and Technology Murthal, India and Dr. (Ms) Manju Arora CSIR-National Physics Laboratory, Dr. K.S. Krishnan Marg, New Delhi, India. Sanjay kumar also acknowledge financial help for National Institute of Technology, Kurukshetra, India.

References

1) M. Sugimoto, "The past, present, and future of ferrites," *J. Am. Ceram. Soc.*, 82 (*2*) 269–280 (1999). doi:10.1111/j.1551-2916.1999.tb20058.x.
2) Y. Iriani, R. Afriani, K. Sandi, and F. Nurosyid, "Co-precipitation synthesis and photocatalytic activity of mn-doped srtio 3 for the degradation of methylene blue wastewater," *Evergr. Jt. J. Nov. Carbon Resour. Sci. Green Asia Strateg.*, 09 1039–1045 (2022). doi.org/10.5109/6625717
3) G. Sachdeva, B. Sharma, P. Anuradha, and S. Verma, "Irreversibility analysis of an ejector refrigeration cycle by modified gouy-stodola formulation," *Evergr. Jt. J. Nov. Carbon Resour. Sci. Green Asia Strateg.*, 10 252–271 (2023). doi.org/10.5109/6781075
4) D. Gaharwar, S. Jha, and B. Kumar Bhuyan, "Fabrication of a hybrid metal matrix composite of al 6082, sic, graphite and mg," *Evergr. Jt. J. Nov. Carbon Resour. Sci. Green Asia Strateg.*, 10 1080–1083 (2023). doi.org/10.5109/6793666
5) A.S. Rini, Y. Rati, R. Fadillah, R. Farma, L. Umar, and Y. Soerbakti, "Improved photocatalytic activity of zno film prepared via green synthesis method using red watermelon rind extract," *Evergr. Jt. J. Nov. Carbon Resour. Sci. Green Asia Strateg.*, 09 1046–1055 (2022). doi.org/10.5109/6625718
6) J. Liu, Z. Jia, W. Zhou, X. Liu, C. Zhang, B. Xu, and G. Wu, "Self-assembled mos2/magnetic ferrite cufe2o4 nanocomposite for high-efficiency microwave absorption," *Chem. Eng. J.*, 429 132253 (2022). doi:10.1016/j.cej.2021.132253.
7) N. Sivakumar, A. Narayanasamy, J.M. Greneche, R. Murugaraj, and Y.S. Lee, "Electrical and magnetic behaviour of nanostructured mgfe2o4 spinel ferrite," *J. Alloys Compd.*, 504 (*2*) 395–402 (2010). doi:10.1016/J.JALLCOM.2010.05.125.
8) K.W. Jung, S. Lee, and Y.J. Lee, "Synthesis of novel magnesium ferrite (mgfe2o4)/biochar magnetic composites and its adsorption behavior for phosphate in aqueous solutions," *Bioresour. Technol.*, 245 751–759 (2017). doi:10.1016/J.BIORTECH.2017.09.035.
9) D. Varshney, and K. Verma, "Substitutional effect on structural and dielectric properties of ni 1-xaxfe2o4 (a = mg, zn) mixed spinel ferrites," *Mater. Chem. Phys.*, 140 (*1*) 412–418 (2013). doi:10.1016/j.matchemphys.2013.03.062.
10) N. Singh, A. Agarwal, and S. Sanghi, "Dielectric relaxation, conductivity behavior and magnetic properties of mg substituted zn-li ferrites," *Curr. Appl. Phys.*, 11 (*3*) 783–789 (2011). doi:10.1016/j.cap.2010.11.073.
11) H. Moradmard, S. Farjami Shayesteh, P. Tohidi, Z. Abbas, and M. Khaleghi, "Structural, magnetic and dielectric properties of magnesium doped nickel ferrite nanoparticles," *J. Alloys Compd.*, 650 116–122 (2015). doi:10.1016/j.jallcom.2015.07.269.
12) K. Verma, A. Kumar, and D. Varshney, "Effect of zn and mg doping on structural, dielectric and magnetic properties of tetragonal cufe2o4," *Curr. Appl. Phys.*, 13 (*3*) 467–473 (2013). doi:10.1016/j.cap.2012.09.015.
13) K. Verma, A. Kumar, and D. Varshney, "Dielectric relaxation behavior of a xco 1-xfe 2o 4 (a = zn, mg) mixed ferrites," *J. Alloys Compd.*, 526 91–97 (2012). doi:10.1016/j.jallcom.2012.02.089.
14) M.K. Hossain, G.F. Ishraque Toki, D.P. Samajdar, M.H.K. Rubel, M. Mushtaq, M.R. Islam, M.F. Rahman, S. Bhattarai, H. Bencherif, M.K.A. Mohammed, R. Pandey, and J. Madan, "Photovoltaic performance investigation of cs3bi2i9-based perovskite solar cells with various charge transport channels using dft and scaps-1d frameworks," *Energy and Fuels*, 37 (*10*) 7380–7400 (2023). doi:10.1021/acs.energyfuels.3c00540/asset/images/medium/ef3c00540_0016.gif.
15) M.K. Hossain, A.A. Arnab, D.P. Samajdar, M.H.K. Rubel, M.M. Hossain, M.R. Islam, R.C. Das, H. Bencherif, M.F. Rahman, J. Madan, R. Pandey, S. Bhattarai, M. Amami, and D.K. Dwivedi, "Design insights into la2nimno6-based perovskite solar cells employing different charge transport layers: dft and scaps-1d frameworks," *Energy and Fuels*, 37 (*17*) 13377–13396 (2023). doi:10.1021/acs.energyfuels.3c02361/asset/images/medium/ef3c02361_0017.gif.
16) M.H.K. Rubel, M.E. Hossain, M.S. Parvez, M.M.

Rahaman, M.S. Islam, N. Kumada, and S. Kojima, "Low-temperature synthesis of potassium triniobate (knb3o8) ceramic powder by a novel aqueous organic gel route," *J. Aust. Ceram. Soc.*, 55 (*3*) 759–764 (2019). doi:10.1007/S41779-018-0287-Z/METRICS.

17) M.H.K. Rubel, M. Mozahar Ali, M.S. Ali, R. Parvin, M.M. Rahaman, K.M. Hossain, M.I. Hossain, A.K.M.A. Islam, and N. Kumada, "First−principles study: structural, mechanical, electronic and thermodynamic properties of simple−cubic−perovskite (ba0.62k0.38)(bi0.92mg0.08)o3," *Solid State Commun.*, 288 22–27 (2019). doi:10.1016/J.SSC.2018.11.008.
18) M.H.K. Rubel, T. Takei, N. Kumada, M.M. Ali, A. Miura, K. Tadanaga, K. Oka, M. Azuma, E. Magome, C. Moriyoshi, and Y. Kuroiwa, "Hydrothermal synthesis, structure, and superconductivity of simple cubic perovskite (ba0.62k0.38)(bi0.92mg0.08)o3 with tc ∼ 30 k," *Inorg. Chem.*, 56 (*6*) 3174–3181 (2017). doi:10.1021/acs.inorgchem.6b01853/suppl_file/ic6b01853_si_002.cif.
19) M. Albino, E. Fantechi, C. Innocenti, A. López-Ortega, V. Bonanni, G. Campo, F. Pineider, M. Gurioli, P. Arosio, T. Orlando, G. Bertoni, C. De Julián Fernández, A. Lascialfari, and C. Sangregorio, "Role of zn2+ substitution on the magnetic, hyperthermic, and relaxometric properties of cobalt ferrite nanoparticles," *J. Phys. Chem. C*, 123 (*10*) 6148–6157 (2019). doi:10.1021/acs.jpcc.8b10998/suppl_file/jp8b10998_si_001.pdf.
20) W.S. Mohamed, M. Alzaid, M.S.M. Abdelbaky, Z. Amghouz, S. García-Granda, and A.M. Abu-Dief, "Impact of co2+ substitution on microstructure and magnetic properties of coxzn1-xfe2o4 nanoparticles," *Nanomater. 2019, Vol. 9, Page 1602*, 9 (*11*) 1602 (2019). doi:10.3390/nano9111602.
21) S. Rana, J. Rawat, M.M. Sorensson, and R.D.K. Misra, "Antimicrobial function of nd3+-doped anatase titania-coated nickel ferrite composite nanoparticles: a biomaterial system," *Acta Biomater.*, 2 (*4*) 421–432 (2006). doi:10.1016/j.actbio.2006.03.005.
22) Y. Matsuo, M. Inagaki, T. Tomozawa, and F. Nakao, "High performance nizn ferrite," *IEEE Trans. Magn.*, 37 (*4 I*) 2359–2361 (2001). doi:10.1109/20.951172.
23) C.F. Rowland, J.M. Pine, E.V.M. Lieven, and A.L. Theakston, "Determinants of acquisition order in wh-questions: re-evaluating the role of caregiver speech," *J. Child Lang.*, 30 (*3*) 609–635 (2003). doi:10.1017/S0305000903005695.
24) B. Ghosh, and A. Gupta, "Effect of nanoribbon width and strain on the electronic properties of the ws2 nanoribbon," *J. Low Power Electron.*, 10 (*3*) 368–372 (2014). doi:10.1166/JOLPE.2014.1345.
25) I. Khishigdemberel, E. Uyanga, H. Hirazawa, and D. Sangaa, "Influence of cu dope on the structural behavior of mgfe2o4 at various temperatures," *Phys. B Condens. Matter*, 544 (*May*) 73–78 (2018). doi:10.1016/j.physb.2018.05.032.
26) O.M. Hemeda, "Electron spin resonance and cation distribution studies of the co0.6zn0.4mnxfe2-xo4 ferrite system," *J. Magn. Magn. Mater.*, 251 (*1*) 50–60 (2002). doi:10.1016/s0304-8853(02)00451-1.
27) S. Thota, S.C. Kashyap, S.K. Sharma, and V.R. Reddy, "Micro raman, mossbauer and magnetic studies of manganese substituted zinc ferrite nanoparticles: role of mn," *J. Phys. Chem. Solids*, 91 136–144 (2016). doi:10.1016/j.jpcs.2015.12.013.
28) K.W. Jung, S. Lee, and Y.J. Lee, "Synthesis of novel magnesium ferrite (mgfe2o4)/biochar magnetic composites and its adsorption behavior for phosphate in aqueous solutions," *Bioresour. Technol.*, 245 751–759 (2017). doi:10.1016/j.biortech.2017.09.035.
29) P. Priyadharsini, A. Pradeep, P.S. Rao, and G. Chandrasekaran, "Structural, spectroscopic and magnetic study of nanocrystalline ni-zn ferrites," *Mater. Chem. Phys.*, 116 (*1*) 207–213 (2009). doi:10.1016/j.matchemphys.2009.03.011.
30) B. Lestriez, A. Maazouz, J.F. Gerard, H. Sautereau, G. Boiteux, G. Seytre, and D.E. Kranbuehl, "Is the maxwell–sillars–wagner model reliable for describing the dielectric properties of a core–shell particle–epoxy system?," *Polymer (Guildf).*, 39 (*26*) 6733–6742 (1998). doi:10.1016/s0032-3861(98)00093-7.
31) A.M.M. Farea, S. Kumar, K.M. Batoo, A. Yousef, C.G. Lee, and Alimuddin, "Structure and electrical properties of co0.5cdxfe2.5-xo4 ferrites," *J. Alloys Compd.*, 464 (*1–2*) 361–369 (2008). doi:10.1016/j.jallcom.2007.09.126.